Comparative classical and '*ab initio*' molecular dynamics study of molten and glassy germanium dioxide

2008 J. Phys.: Condens. Matter 20 285106

(http://iopscience.iop.org/0953-8984/20/28/285106)

J. Phys.: Condens. Matter **20** (2008) 285106 (15pp) doi:10.1088/0953-8984/20/28/285106

Comparative classical and '*ab initio*' molecular dynamics study of molten and glassy germanium dioxide

M Hawlitzky[1], J Horbach[1,2], S Ispas[3], M Krack[4] and K Binder[1]

[1] Institut für Physik, Johannes Gutenberg-Universität Mainz, Staudinger Weg 7, 55099 Mainz, Germany
[2] Institut für Materialphysik im Weltraum, Deutsches Zentrum für Luft- und Raumfahrt (DLR), 51170 Köln, Germany
[3] Laboratoire des Colloïdes, Verres et Nanomatériaux, Université Montpellier II and CNRS UMR 5587, 34095 Montpellier, France
[4] Computational Science, Department of Chemistry and Applied Biosciences, ETH Zürich, USI Campus, Via Giuseppe Buffi 13, 6900 Lugano, Switzerland

E-mail: juergen.horbach@dlr.de and kurt.binder@uni-mainz.de

Received 19 February 2008, in final form 16 May 2008
Published 13 June 2008
Online at stacks.iop.org/JPhysCM/20/285106

Abstract

A molecular dynamics (MD) study of the static and dynamic properties of molten and glassy germanium dioxide is presented. The interactions between the atoms are modeled by the classical pair potential proposed by Oeffner and Elliott (OE) (1998 *Phys. Rev.* B **58** 14791). We compare our results to experiments and previous simulations. In addition, an '*ab initio*' method, the so-called Car–Parrinello molecular dynamics (CPMD), is applied to check the accuracy of the structural properties, as obtained by the classical MD simulations with the OE potential. As in a similar study for SiO_2, the structure predicted by CPMD is only slightly softer than that resulting from the classical MD. In contrast to earlier simulations, both the static structure and dynamic properties are in very good agreement with pertinent experimental data. MD simulations with the OE potential are also used to study the relaxation dynamics. As previously found for SiO_2, for high temperatures the dynamics of molten GeO_2 is compatible with a description in terms of mode coupling theory.

(Some figures in this article are in colour only in the electronic version)

1. Introduction

Understanding the structure and dynamics of glassforming fluids and the nature of the glass transition is one of the most challenging unsolved problems of the physics of condensed matter [1–7]. One of the most debated issues is the question to what extent the glass transition is a universal phenomenon; i.e. it is debated whether the mechanisms causing the dramatic slowing down in undercooled fluids when the glass transition is approached are basically the same in all glassforming materials, or whether qualitatively different classes of glass transitions exist, similar to the 'universality classes' of critical phenomena [8].

One such distinction in two classes has been proposed by Angell [9], namely the distinction between 'strong' and 'fragile' glassformers. Plotting the logarithm of the viscosity $\eta(T)$ versus the normalized inverse temperature T_g/T (the glass transition temperature T_g is here defined somewhat arbitrarily from the condition $\eta(T = T_g) = 10^{13}$ Poise), one observes that certain network-forming materials such as molten SiO_2 and molten GeO_2 simply follow straight lines, i.e. the temperature dependence of $\eta(T)$ can be described by an Arrhenius law,

$$\eta(T) = \eta_\infty \exp(E_a/k_B T), \tag{1}$$

where η_∞ is a constant and E_a plays the role of an activation energy. However most other glassforming systems, in particular polymer melts, multicomponent metallic melts, and fluids formed from small organic molecules, behave differently. For these glassformers, the plot of $\log[\eta(T)]$ versus

T_g/T is strongly curved. Following Angell [9], these systems are called 'fragile glassformers'.

There is ample evidence [6, 10] that in fragile glassformers the initial stages of slowing down, when the structural relaxation times grow from the picosecond scale by several orders of magnitude, can be described rather well by mode coupling theory (MCT) [3], although some aspects of this theory are still under discussion [11], and there is no consensus on the behavior near T_g [6, 12–14]. For the case of silica, computer simulation studies [15–17] have shown that the relaxation dynamics at high temperatures can be well described by MCT, whereas at low temperatures an Arrhenius behavior is observed, as seen in experiments (note that the high temperature regime is almost inaccessible to experiment). This indicates that, at least on a qualitative level, the 'strong glassformer' SiO_2 exhibits a similar behavior for the temperature dependence of transport coefficients and structural relaxation as typical 'fragile glassformers'. Now, the question arises whether this is also true for the other prototype of a 'strong glassformer', namely GeO_2. While molten silica has been studied extensively, both by various experimental techniques and by computer simulations [15–35], there are fewer studies of molten and glassy germanium dioxide, and this holds true for both experiments [36–47] and simulations [48–57].

In the present work, we hence present a detailed molecular dynamics (MD) [58, 59] study of molten and glassy GeO_2 at zero pressure, using a pair potential model that has been recently proposed by Oeffner and Elliott [48]. In order to check whether the Oeffner–Elliott (OE) potential provides a chemically realistic modeling of GeO_2, we perform also '*ab initio*' Car–Parrinello molecular dynamics (CPMD) simulations [60–62] and compare various structural and dynamic quantities as obtained from classical MD using the OE potential with those from the CPMD calculations. Moreover, our simulation results are also validated by comparison to experimental data.

In section 2 we summarize the models and methods of the simulation, while section 3 is devoted to a description of the static properties of molten and glassy GeO_2 (partial pair distribution functions and structure factors, ring statistics and angular distributions, etc). Section 4 presents selected information on dynamic properties (mean square displacements, intermediate incoherent scattering functions), while section 5 summarizes some conclusions.

2. Models and simulation methods

2.1. Classical MD

In a classical MD simulation, all degrees of freedom due to the electrons are disregarded, as well as quantum effects due to the ions (which need to be included for a correct description of thermal properties of glasses at temperatures far below the glass transition temperature). One simply solves Newton's equations of motion, which is conveniently done applying the velocity form of the Verlet algorithm [58, 59]. Forces are computed using the OE potential [48],

$$V_{\alpha\beta}(r_{ij}) = \frac{q_\alpha q_\beta e^2}{r_{ij}} + A_{\alpha\beta}\exp(-B_{\alpha\beta}r_{ij}) - C_{\alpha\beta}r_{ij}^{-6} \qquad \alpha, \beta \in \mathrm{Ge, O}. \tag{2}$$

Here, $r_{ij} = |\vec{r}_i - \vec{r}_j|$ is the distance between a pair of particles at positions $\vec{r}_i$ and $\vec{r}_j$. The first term on the right-hand side of equation (2) describes Coulomb interactions, with e the elementary charge and the values $q_{Ge} = 1.5$ and $q_O = -0.75$ for the partial charges of germanium and oxygen ions, respectively [48]. The second and third term in (2) form a Buckingham potential and describe the short-range part of the potential. The constants $A_{\alpha\beta}$, $B_{\alpha\beta}$ and $C_{\alpha\beta}$ are [48] $A_{GeO} = 208\,011.52$ eV, $B_{GeO} = 6.129\,329$ Å^{-1}, $C_{GeO} = 236.653$ eV Å^6, $A_{OO} = 7693.522$ eV, $B_{OO} = 3.285\,108$ Å^{-1}, and $C_{OO} = 131.09$ eV Å^6. The Buckingham terms for the Ge–Ge interaction are set to zero. The OE potential was derived from quantum-chemical calculations of GeO_4 tetrahedra, also using experimental data from the α-GeO_2 crystal structure at $T = 300$ K as input information. We note that analogous procedures for the chemically similar case of SiO_2 have led to the potential due to van Beest, Kramer and van Santen ('BKS potential') [63], which has proven useful in reproducing a great variety of experimental results rather accurately [15, 22, 25, 26, 30]. Note that for SiO_2 the effective charges are different ($q_{Si} = 2.4$, $q_O = -1.2$), despite the chemical similarity. Thus, a combination of the OE and the BKS potential would not be suitable for the description of oxide melts containing both GeO_2 and SiO_2, since the O–O interaction is modeled differently in both cases.

Several other potential models have been proposed in the literature [52, 64, 65], but structural properties of liquid GeO_2 derived from these potentials are not in good agreement with experiment, and hence these potentials were not used in the present study.

While the short-range part of equation (1) was cut off and shifted to zero at a distance $r_c = 7.5$ Å [66], the long-range Coulomb interactions were treated by Ewald summation methods [58, 66]. The equations of motion were solved for systems of $N = 1152$ atoms using an integration time step of 1.23 fs and periodic boundary conditions in all three spatial directions. The simulations in the NpT ensemble at constant zero pressure, $p = 0$, yielded linear dimensions $L(T)$ of the cubic simulation box in the range 26.6 Å $\leqslant L(T) \leqslant$ 28.4 Å for temperatures in the range 2530 K $\leqslant T \leqslant$ 6100 K. Pressure was kept constant using an Andersen barostat, using a value of 8×10^{-3} u for the mass of the piston [68]. Constant temperature was realized by coupling the system periodically (i.e. every 0.18 ps) to a stochastic heat bath [58]. Note that the runs in the NpT ensemble were only used to create well-equilibrated initial configurations for runs in the microcanonical NVE ensemble (V denoting the system volume and E its internal energy). Using force parallelization with message passing interface (MPI) routines, an efficient use of the Jülich multiprocessor system (JUMP) with 32 processors used in parallel was possible. Equilibration times t_e spanned the range from 48.9 ps (40 000 time steps) at $T = 6100$ K to 11.97 ns (almost 10^7 time steps) at $T = 2530$ K, to generate

8 initial configurations, which were then propagated in the NVE ensemble for the same time interval t_e, during which structural and dynamical properties were recorded. Note that the time t_e was chosen such that the slower species (Ge) moved on average a distance of 5.5 Å at each temperature. Further implementation details are documented in [66].

2.2. CPMD

Car–Parrinello molecular dynamics (CPMD) simulations [60, 61] of GeO_2 have been performed, using the CPMD software [62]. In CPMD, the electronic degrees of freedom are treated in the framework of density functional theory, in this work within the general gradient approximation (GGA). An important issue for CPMD is the quality of the pseudopotentials, which are a necessary input for any *ab initio* calculation that does not take into account the electronic degrees of freedom of all the electrons of an atom, but only the valence electrons. While we found that a pseudopotential due to Goedecker *et al* [69] was computationally too demanding for our purposes, a pseudopotential with the BLYP exchange–correlation functional in the Troullier–Martins parametrization [70] was found to be satisfactory. As an energy cut-off for the plane waves $E_{cut} = 75$ Ryd was used, similar to in related work for SiO_2 [28]. The time step was 0.0726 fs. For the thermostatting of the system, we used Nosé–Hoover chains [71] for each ionic degree of freedom as well as for the electronic degrees of freedom to counterbalance the energy flow from ions to electrons [72]. The parameters used for the Nosé–Hoover chains can be found in a previous publication [29].

An important problem in CPMD simulations of amorphous systems is the generation of suitable initial configurations. While in the case of SiO_2, it was found useful to start from classical MD simulations using the BKS potential [63] and relax these configurations to new equilibrium states by CPMD [28, 73, 74], in the case of GeO_2 (using the OE potential [48]) such a procedure did not converge [66]. The reason for this failure is that the differences between equilibrated atomic configurations using either classical MD or CPMD methods for GeO_2 are slightly larger than for SiO_2, as far as interatomic distances, angles etc are concerned. At the temperatures of interest ($T = 3760$ and 3000 K), which are far above the melting temperature T_m of GeO_2 ($T_m = 1389$ K [75]) it is also too time-consuming to start from a crystalline configuration and melt it in a CPMD run; thus we decided to start from configurations generated by classical MD at $T = 7000$ K, where subsequent equilibration by CPMD turned out to be feasible (for 60 particles this took 53 000 CPMD steps, while for 120 particles 21 000 CPMD steps were sufficient, using periodic boundary conditions throughout). Then the temperature was lowered in a single step to $T = 3760$ K (for $N = 60$) or $T = 3000$ K (for $N = 60$ and 120), respectively. At $T = 3760$ K, runs over 171 000 time steps for equilibration and production were performed corresponding to a real time of 12.4 ps. At $T = 3000$ K, we did runs over 340 000 time steps for the system with 60 particles and 420 000 time steps for the system with 120 particles, thus covering a time range of 24.7 ps and 30.5 ps, respectively. In order to obtain better statistics, we averaged over 6 independent simulation runs for each system size and temperature considered.

The density was chosen to be $\rho = 3.45$ g cm^{-3}, similar to the equilibrium density resulting from the classical MD simulations in this temperature range, in order to be able to compare MD and CPMD results at essentially the same density. This choice implies linear dimensions of the simulation box of $L = 10.023$ Å for $N = 60$ and $L = 12.629$ Å for $N = 120$. Since the periodic boundary condition does significantly affect the structure and correlation functions for distances that exceed $L/2$, the smallness of N and L is clearly a major disadvantage of our implementation of CPMD, and prevents us from a meaningful study of intermediate range order by CPMD. The application of novel versions of *ab initio* MD, suitable to simulate significantly larger systems [76], is desirable, but must be left to future work.

Finally, we mention that sometimes the generated configurations had to be discarded 'by hand', when they contained well-identifiable O_2 molecules disjunct from the remaining germanium oxide network (which then, of course, necessarily has coordination defects). It is clear that at $T = 7000$ K such chemical disintegration of GeO_2 may be a physically meaningful effect. But we are interested in the properties of GeO_2 at lower temperatures, where these separate O_2 molecules should no longer occur, but rather should be reintegrated into the network structure. However, experiments by Vergano and Uhlmann [77] have found evidence for the occurrence of O_2 molecules in germania melts above about 1500 K. But since the occurrence of O_2 molecules in the CPMD is probably a result of the preparation of our samples, we prefer here to select only configurations without O_2 molecules for the analysis.

With respect to other implementation details, we closely followed the procedures of Benoit *et al* [29] (see also [66]). We only note that, in our case, the CPU time required for the CPMD is a factor of 358 000 higher than that needed for the classical MD, using the same multiprocessor system and the same system size for both methods [66]. Therefore, only a rather restrictive use of CPMD was feasible.

3. Static properties of molten and glassy GeO_2

As discussed in section 2.1, equilibration was done in the framework of classical MD using the NpT ensemble which allows us to record the temperature dependence of the density (figure 1). In our MD simulation, the lowest temperature which could still be equilibrated with manageable effort was $T = 2530$ K. This temperature corresponds to almost twice the melting temperature [75], while experimental data are only available at much lower temperatures. Therefore, we used states at $T = 2750$ K for further cooling down of the samples (note that the states at $T = 2530$ K were not yet available when these cooling runs were performed). To this end, temperature was linearly decreased according to

$$T(t) = 2750\ \text{K} - Qt, \tag{3}$$

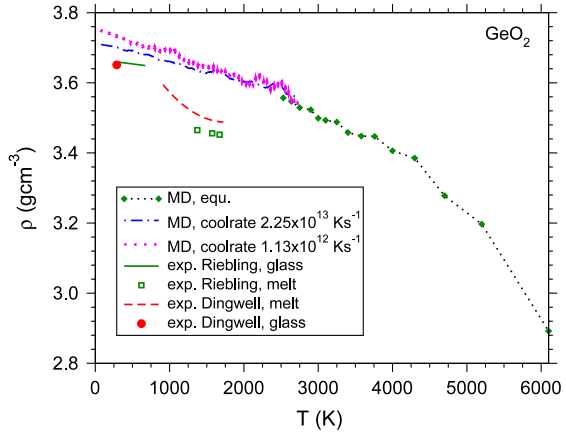

Figure 1. Density of GeO_2 plotted versus temperature. Well-equilibrated MD results (diamonds), using the OE potential, are shown in the temperature range 6100 K $\geqslant T \geqslant$ 2530 K. The dotted line connecting the data points serves only as a guide to the eye. The MD data shown for $T < 2750$ K result from cooling runs with two different cooling rates, using well-equilibrated configurations at $T = 2530$ K as a starting point (cf equation (3)). All the simulation results were obtained at zero pressure. Experimental data from Riebling [36] and Dingwell *et al* [39] are shown for comparison.

with cooling rates $Q = 2.25 \times 10^{13}$ and 1.13×10^{12} K s^{-1}. As in the case of SiO_2 [15, 22], the cooling rates available in MD exceed those of the experiment by many orders of magnitude, and a meaningful extrapolation to these very small experimental cooling rates is not possible. Although the presence of a density maximum (as is known to occur in SiO_2 [78]) somewhere around $T = 2000$ K cannot be excluded, it seems very unlikely that for slow cooling rates the simulated densities for $T \leqslant 1700$ K would decrease enough to match the experimental data. So we attribute the larger part of the mismatch between simulated and experimental melt densities to the inadequacy of the OE potential to predict the density very accurately. However, such a 5% discrepancy in the density is not uncommon when classical pair potentials are used.

Surprisingly, at $T = 300$ K the experimental density is $\rho_{\text{exp}} \approx 3.65$ g cm^{-3} and the simulated one (with the slowest of our cooling rates) $\rho_{\text{sim}} \approx 3.70$ g cm^{-3}, thus only 1.37% higher. However, this good agreement is presumably due to a lucky cancelation of errors (freezing in a too high density due to the inaccurate potential, partially compensates for not reproducing the rapid variation of the density of supercooled GeO_2 around $T = 1000$ K due to our excessively rapid cooling). This example again shows that fits or misfits of isolated experimental data points by simulations are unsuitable to judge the quality of potentials and/or simulation procedures.

Further information on the static structure are provided by the static structure factor. Note that this quantity can be measured using neutron scattering techniques. Since we deal here with two species, it is appropriate to consider partial structure factors $S_{\alpha\beta}(q)$ ($\alpha, \beta =$ Ge, O)

$$S_{\alpha\beta}(q) = \frac{1}{N}\left\langle \sum_{i=1}^{N_\alpha}\sum_{j=1}^{N_\beta} \exp(\mathrm{i}\vec{q}\cdot\vec{r}_{ij})\right\rangle, \qquad (4)$$

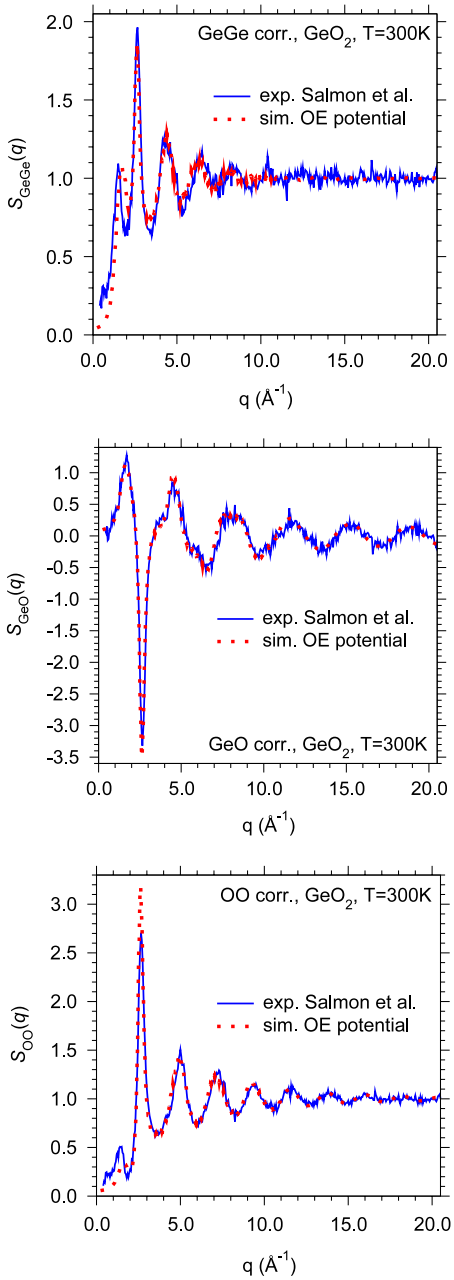

Figure 2. Partial neutron scattering structure factors $S_{\alpha\beta}(q)$ plotted versus wavenumber q, comparing the present MD simulation to the experimental data of Salmon *et al* [46, 47] at $T = 300$ K.

where N_α (N_β) corresponds to the number of particles of species α (β) = Ge, O. Note that fluids and glasses are isotropic and hence $S_{\alpha\beta}(q)$ depends only on the absolute value $q = |\vec{q}|$ and not on the direction of the scattering vector $\vec{q}$. Using suitable isotopes, all partial structure factors for GeO_2 have recently been measured by Salmon *et al* [46, 47]. Figure 2 reveals an overall good agreement between our simulation results and these data. However, there are discrepancies at small q ($q < 2$ Å^{-1}) that indicate that the intermediate range order in GeO_2, as seen by the OE potential, exhibits differences to that, as found by experiment. This observation is in agreement with recent studies, comparing simulations with the OE potential to experiment [46, 57].

Standard neutron scattering yields a scattering intensity weighted with the scattering lengths b_α, b_β as follows

$$S(q) = \frac{N}{\sum_\alpha N_\alpha b_\alpha^2} \sum_{\alpha,\beta\in\{\mathrm{Ge,O}\}} b_\alpha b_\beta S_{\alpha\beta}(q). \qquad (5)$$

Using[5] $b_{\mathrm{Ge}} = 8.185$ fm, $b_{\mathrm{O}} = 5.803$ fm one can compute from equations (4) and (5) the neutron scattering structure factor from the simulation and compare it to the corresponding experimental data [43] without any adjustable parameters whatsoever. Also for this comparison [51, 67] the general agreement between simulation and experiment is rather good; both predict a 'first sharp diffraction peak' (FSDP) [1, 6, 79] at about $q_{\max} \approx 1.55$ Å^{-1}, which can be attributed in real space to the linear dimension of two GeO_4 tetrahedra sharing a corner (see below), $\ell = 2\pi/q_{\max} \approx 4.05$ Å.

When we compare to SiO_2 [15, 80] we note that in SiO_2 the FSDP occurs at a slightly larger value, $q_{\max} \approx 1.7$ Å^{-1}, implying a somewhat smaller linear dimension of the two corner-sharing SiO_4 tetrahedra (note that the 'chemical rules' [1] for the formation of perfect binary continuous random networks, with a cation in the center of a tetrahedron and oxygens at the corners, such that each oxygen is shared by two neighboring tetrahedra, are identical for SiO_2 and GeO_2). But a more interesting difference is the fact that SiO_2 shows a second well-developed peak, at about $q'_{\max} \approx 3$ Å^{-1}, which corresponds to a peak in GeO_2 at about $q'_{\max} \approx 2.6$ Å^{-1}. While in the total neutron scattering structure factor this peak is hardly distinguishable from the noise, the partial static structure factors figures 2 and 3 reveal that actually this is the main peak in the structure, corresponding to a distance $\ell' = 2\pi/q'_{\max} \approx 2.4$ Å. This distance is similar to the base to apex distance in a regular tetrahedron [47], $4r_{\mathrm{GeO}}/3 \approx 2.33$ Å (with $r_{\mathrm{GeO}} = 1.75$ Å the average length of a GeO bond, see below). In real space, i.e. in the partial pair distribution functions $g_{\alpha\beta}(r)$, the peaks in the partial static structure factors are reflected by oscillations with a rapidly decreasing amplitude at large distances (figure 4). These correlations are obtained from the simulated configurations, using the definition

$$g_{\alpha\beta}(r) = \mathcal{N}_{\alpha\beta} \left\langle \sum_{i=1}^{N_\alpha} \sum_{j=1}^{N_\beta} \frac{1}{4\pi r^2} \delta(r - |\vec{r}_i - \vec{r}_j|) \right\rangle, \quad \alpha, \beta = \{\mathrm{Ge, O}\}, \qquad (6)$$

where $\mathcal{N}_{\alpha\beta} = V/(N_\alpha N_\beta)$ if $\alpha \neq \beta$ while $\mathcal{N}_{\alpha\alpha} = V/[N_\alpha(N_\alpha - 1)]$, V being the volume of the simulation box. The correlation functions $g_{\alpha\beta}(r)$ and $S_{\alpha\beta}(q)$ are related via [6, 81]

$$S_{\alpha\beta}(q) = 1 + (N/V) \int [g_{\alpha\beta}(\vec{r}) - 1] \exp(\mathrm{i}\vec{q}\cdot\vec{r})\, \mathrm{d}\vec{r}. \qquad (7)$$

In the following, we shall focus on $g_{\alpha\beta}(r)$ rather than on $S_{\alpha\beta}(q)$. Figure 4 shows the $g_{\alpha\beta}(r)$ from the simulation for the melt at 4300 and 2530 K as well as for the glass at 300 K. Also included in the figure are the experimental $g_{\alpha\beta}(r)$ at room temperature, as measured by Salmon *et al* [46]. As expected from figure 2, the largest discrepancies between simulation and experiment can be seen in $g_{\mathrm{GeGe}}(r)$, where in particular the shape of the first and the second peak is different in the experimental data. However, the location of the first peaks in $g_{\alpha\beta}(r)$ and the average coordination numbers $z_{\alpha\beta}$ show an overall good agreement with experiment (see table 1). Note that the coordination number $z_{\alpha\beta}$ is the number of nearest neighbors of type β around a particle of type α. For the cut-off distances defining nearest neighbors we have chosen 3.68 Å, 2.0 Å and 3.15 Å for the GeGe, GeO and OO correlations, respectively. These cut-off distances correspond to the minima in the corresponding partial pair distribution functions.

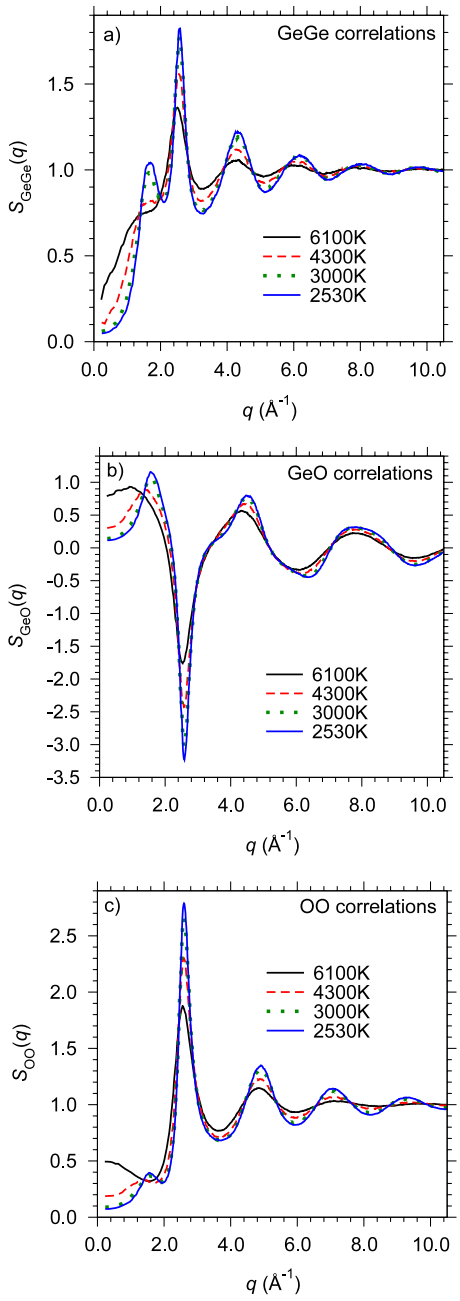

Figure 3. Partial structure factors $S_{\mathrm{GeGe}}(q)$, part (a), $S_{\mathrm{GeO}}(q)$, part (b), and $S_{\mathrm{OO}}(q)$, part (c), plotted versus q and four temperatures, as indicated.

[5] See NIST Neutron Scattering lengths and CrossSections available at http://www.ncnr.rist.gov/resources/n-lengths/.

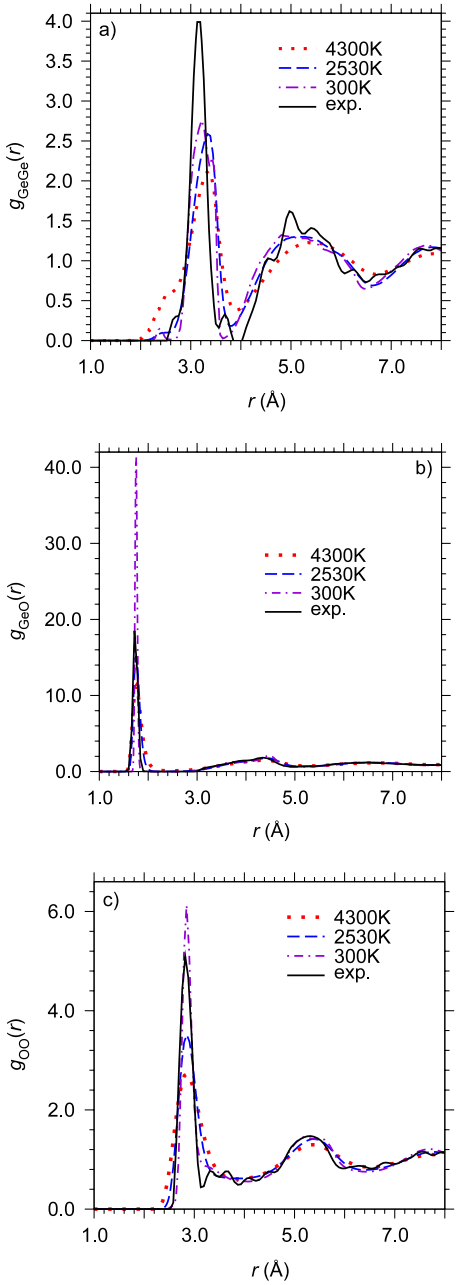

Figure 4. Partial pair distribution functions $g_{\alpha\beta}(r)$ for GeO_2 plotted versus r for liquid GeO_2 at 4300 and 2530 K as well as for glassy GeO_2 at 300 K, as obtained from classical MD. Also included are experimental results by Salmon *et al* [46], as determined from Fourier transforms of measured partial static structure factors at room temperature.

As we can infer from figure 4, the first peak in $g_{GeO}(r)$ is a factor of two higher in the simulation than in the experiment. Moreover, the average coordination number z_{GeO} is significantly below 4 in the experiment whereas it is slightly above 4 in the simulation (table 1). This is surprising regarding the good agreement of the partial structure factors for the GeO correlations. However, one has to keep in mind that the experimental $g_{\alpha\beta}(r)$ are affected by the q space resolution function of the instrument used to measure the diffraction data (see appendix C of [83]). The resolution function will have a particularly severe effect on the height of the first Ge–O peak (the nearest-neighbor distance is relatively short and the spread of nearest-neighbor distances is small) and leads to a reduction from 4 in the Ge–O coordination number. Note that the Ge–O distance (about 1.75 Å) clearly is the smallest distance occurring in the structure, and the sharpness of this peak (note the ordinate scale of figure 4(b) in comparison to that of figure 4(a)) reveals that the GeO_4 tetrahedra are fairly rigid. Only for the Ge–Ge distance a slight systematic discrepancy between MD and experiment is visible. Comparing to the CPMD results (figure 5), however, this discrepancy seems to be removed.

Table 1. Positions of the first peaks in $g_{\alpha\beta}(r)$ and the average coordination numbers $z_{\alpha\beta}$ for the $\alpha\beta$ correlations. The results from the classical MD simulation at 300 K are compared to experimental values [47].

	r_{GeGe} (Å)	r_{GeO} (Å)	r_{OO} (Å)	z_{GeGe}	z_{GeO}	z_{OO}
Sim.	3.22	1.75	2.85	4.15	4.01	6.62
Exp. [47]	3.16	1.73	2.83	4.1	3.8	6.7

We have also compared CPMD results for $S_{\alpha\beta}(q)$ and $S(q)$ with the corresponding MD results [66]; these comparisons strengthen the conclusion that one can also draw from figure 5, namely that MD yields a rather accurate description of the local structure of molten GeO_2. Note that slight discrepancies in $g_{OO}(r)$ for $r > 5$ Å should not be taken very seriously, because at these distances CPMD suffers from finite size effects, as noted above. More interesting is the difference (emphasized in the inset of figure 5(c)) concerning the feature near 1.5 Å. Testing carefully different equilibration times it was possible to show that the prepeak in $g_{OO}(r)$ has a larger amplitude if the equilibration time is too short [66]. Therefore, this difference between the CPMD and the MD results is probably a real effect, at least it is not an artifact of too short equilibration. Of course, one can question the accuracy of CPMD somewhat on other grounds: other '*ab initio*' studies of the GeO_2 structure [51, 82] using different pseudopotentials and system preparation procedures predicted somewhat different results (e.g. the Ge–O distance $r_{GeO} = 1.69$ Å [82] or $r_{GeO} = 1.78$ Å [51], while we obtain 1.71 Å and the experimental value is 1.73 ± 0.03 Å [40, 45]).

We now turn our attention to the analysis of structural features on intermediate length scales. To this end, we recall the concept of 'ring statistics' [6, 22]. One considers the shortest closed paths in the network of covalent bonds, starting from an oxygen atom (figure 6). The length n of a ring is then the number of cations (Ge in the present case, or Si in the case of silica [22]) that one passes before one returns to the starting point. Figure 6 shows, as an example, $n = 6$ (left) and $n = 2$ (middle part). In SiO_2 (both in the bulk and at free surfaces to vacuum), it has been found that the angles between atoms in a ring with $n = 2$ and 3 differ appreciably between the classical MD simulation and its CPMD counterpart [73, 74], and this also significantly affects the probability $P(n)$ that a ring of length n occurs in the structure (in thermal equilibrium). At first sight one might conclude that a similar effect occurs

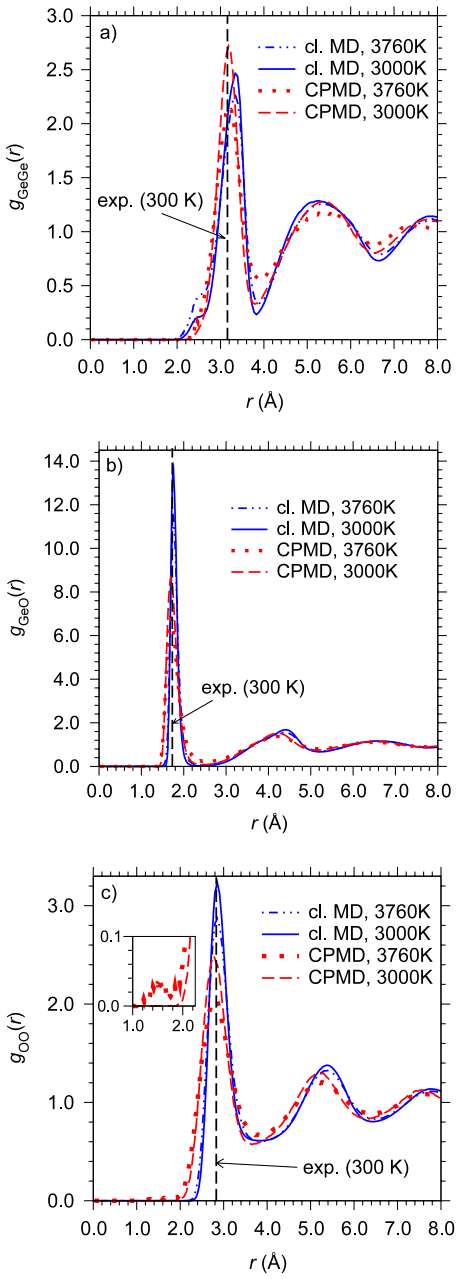

Figure 5. Partial pair distribution functions $g_{\alpha\beta(r)}$ for GeO_2 plotted at $T = 3000$ and 3760 K, comparing classical MD with CPMD. Also the experimental values for the nearest-neighbor distance at $T = 300$ K are included [46]. The inset in the oxygen–oxygen correlation (part (c)) shows a magnified view of the side maximum appearing around $r \approx 1.5$ Å.

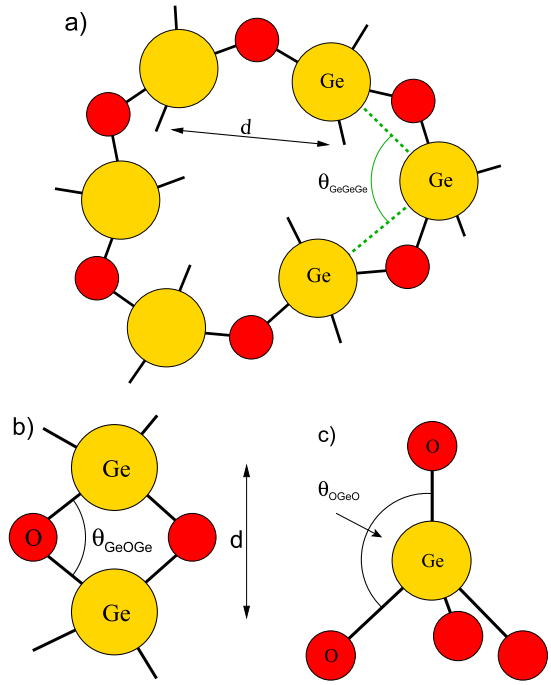

Figure 6. Schematic picture of a ring of length $n = 6$, illustrating also the definition of the angle θ_{GeGeGe} and the distance d between neighboring Ge atoms (a). A ring of length $n = 2$ and the angle θ_{GeOGe} is sketched in (b), and the tetrahedral angle θ_{OGeO} in (c).

for GeO_2 as well (figure 7(a)), but a closer analysis reveals that most of the differences between CPMD and MD stem from the fact that the former suffers from finite size effects (figure 7(b)): when we use $N = 60$ in the MD calculation, we find almost perfect agreement with the CPMD calculation that uses $N = 60$ as well. Also the strong difference between the CPMD results for $N = 60$ and 120 show that one cannot trust the CPMD results for $P(n)$, due to these dominant finite size effects. Clearly, for a quantity that depends sensitively on the order of intermediate length scales like $P(n)$ it is more important to choose a large enough system rather than to work with very realistic descriptions of the forces, as provided by CPMD.

Hence while CPMD is less useful for the study of properties that depend sensitively on medium range order, it clearly is of great interest for the assessment of local properties, such as the distributions of angles between the 'bonds' in the structure. These distributions have also been obtained by MD for a wide range of temperatures (figure 8). The definition of the Ge–Ge–Ge angle is indicated in figure 6(a); other angles are defined analogously. A remarkable feature is that all distributions, with the exception of the tetrahedral angle O–Ge–O, have a double peak shape, and are rather broad. Only the distribution of the tetrahedral angle tends towards a Gaussian shape, as the temperature is lowered, and gets somewhat sharper; in a random network structure formed by ideal tetrahedra only, this distribution would be a delta function, $\delta(\theta - \theta_{tetr})$ with $\theta_{tetr} = 109°$.

The relative weight of the peak at $\theta = 60°$ of the Ge–Ge–Ge angle decreases with decreasing temperature, as well as the weight of the peak at $\theta = 90°$ for the Ge–O–Ge angle distribution. A consideration of the geometry of the rings (figure 6) immediately shows that the peak of $P(\theta)$ for the Ge–Ge–Ge angle can be attributed to rings with $n = 3$, and similarly the peak of $P(\theta)$ for the Ge–O–Ge angle at $\theta = 90°$ is due to rings with $n = 2$. Such small rings can be frequently observed in the structure of GeO_2 at high temperatures, while at low temperatures the network becomes much more regular, and the density of all small rings decreases significantly.

For $T = 2530$ K, the position of the main peak of the distribution $P(\theta)$ for the Ge–O–Ge angle is 133°. It is

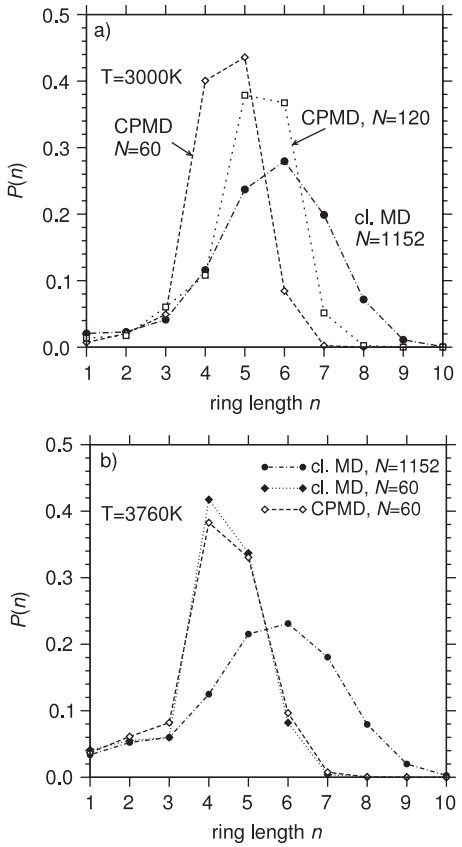

Figure 7. Probability $P(n)$ that a ring of length n occurs, plotted versus n, for $T = 3000$ and 3760 K, comparing MD and CPMD (a), and the same comparison including an MD study where $N = 60$, as in the CPMD calculation (b).

gratifying that this number coincides with the corresponding experimental estimates [40, 84]. This agreement is a further indication that the OE potential is able to provide a rather realistic description of the structure.

The side peaks of figures 8(a) and (b), tend to disappear at physically relevant temperatures, i.e. the number of rings with $n = 2$ and 3 becomes significantly smaller with decreasing temperature. This is also revealed by the temperature dependence of the ring length distribution $P(n)$, indicating that the small rings essentially do not persist into the glass phase [66]. The main peaks of the GeGeGe and GeOGe distributions seem to stay rather broad, as expected due to the disorder in the network structure. Only in the various crystal structures of GeO_2 at low temperatures we would expect very sharp distributions of all angles; in the glass structure only the distributions of the angles inside a tetrahedron become rather sharp at low temperatures.

In this respect, the distribution of the angle θ between O–O–O bonds is special: figure 8(d) shows that two peaks occur, which clearly persist at low temperatures. The obvious explanation is that there are two distinct possibilities: the peak at $\theta = 60°$ can be attributed to oxygen atoms belonging to the same tetrahedron, while the peak at $\theta \approx 110°$ is due to oxygens belonging to two neighboring tetrahedra. In fact, as the temperature decreases the structure of a single tetrahedron approaches closer and closer to that of an ideal tetrahedron, whose faces are perfect triangles, having angles of 60°. In view of this, the observation that the peak at $\theta = 60°$ becomes clearly sharper with decreasing temperature is not surprising.

Now we turn to the comparison of these angular distributions to the corresponding CPMD predictions (figure 9). The general shape of these distributions is very similar, with the exception of the Ge–O–Ge angle, where the side peak at 90° (due to rings with $n = 2$) is broadened into a shoulder only, indicating that the OE potential overestimates in particular the rigidity of this structural element (a schematic picture of a ring with $n = 2$ is shown in figure 6(b)). We also note that the CPMD distributions are always somewhat broader than the MD results at the corresponding temperature. This indicates that the CPMD calculation, if we could parametrize it in terms of an effective pair potentials having the OE or BKS form, would yield a systematically softer potential. In fact, if one compares the CPMD calculation at $T = 3000$ K to the classical calculation at $T = 3760$ K, the differences are much smaller [66]. Of course, we do not wish to imply that the differences between CPMD and MD could be fully eliminated by a renormalization of the temperature scale: for the main peak of the Ge–O–Ge angle distribution, CPMD at $T = 3000$ K implies a peak at about 129°, while the MD calculation yields a peak at about 133° (this value depends much less on temperature than the CPMD peak position does). We have also done MD simulations with $N = 60$ particles only, to rule out that the differences seen in figure 9 are simply due to finite size effects [66]. Figure 9(a) also indicates for the Ge–Ge–Ge distribution that the CPMD result for $N = 60$ is only slightly different from that at $N = 120$ (for the other distributions the differences are even smaller).

As a conclusion of this section we may state that the OE potential predicts slightly too rigid structures in comparison to CPMD, and this difference is most pronounced at rather high temperatures. However, the overall agreement between the structure as predicted by the OE potential and the structure resulting from CPMD is very good. The same conclusion also emerges from an analysis of the distribution of coordination numbers [66]. The comparison to experimental data, whenever available, also suggests the statement that the OE potential provides a reasonably accurate description of the static structure of molten and glassy GeO_2.

4. Dynamic properties of GeO_2 melts

From the MD runs in the *NVE* ensemble, it is straightforward to record both the mean square displacements (MSD) of a tagged particle of type α ($\alpha = \{\mathrm{Ge}, \mathrm{O}\}$) [4, 6, 81],

$$\langle r_\alpha^2(t)\rangle = \frac{1}{N_\alpha}\sum_{i=1}^{N_\alpha}\langle|\vec{r}_i(t) - \vec{r}_i(0)|^2\rangle, \tag{8}$$

and the intermediate incoherent scattering function

$$F_s^\alpha(q,t) = \frac{1}{N_\alpha}\sum_{i=1}^{N_\alpha}\langle\exp\{-\mathrm{i}\vec{q}\cdot[\vec{r}_i(t) - \vec{r}_i(0)]\}\rangle. \tag{9}$$

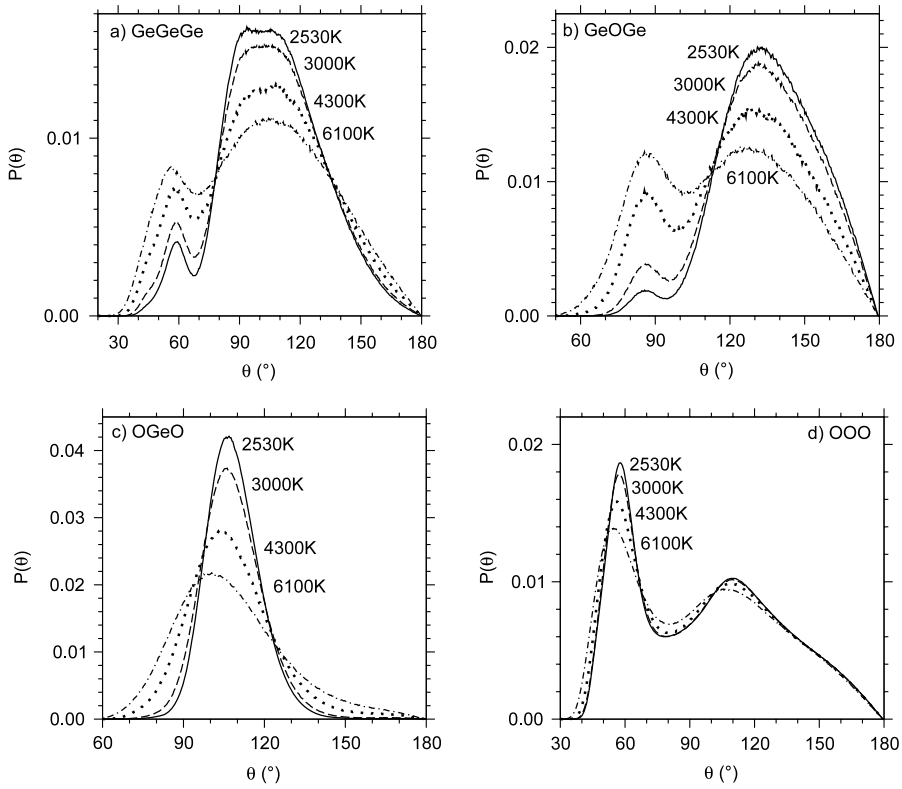

Figure 8. Distribution functions $P(\theta)$ of various angles θ, obtained from MD for a wide range of temperatures, as indicated. Case (a) shows the Ge–Ge–Ge angle, case (b) the Ge–O–Ge angle, case (c) the O–Ge–O angle and case (d) the O–O–O angle.

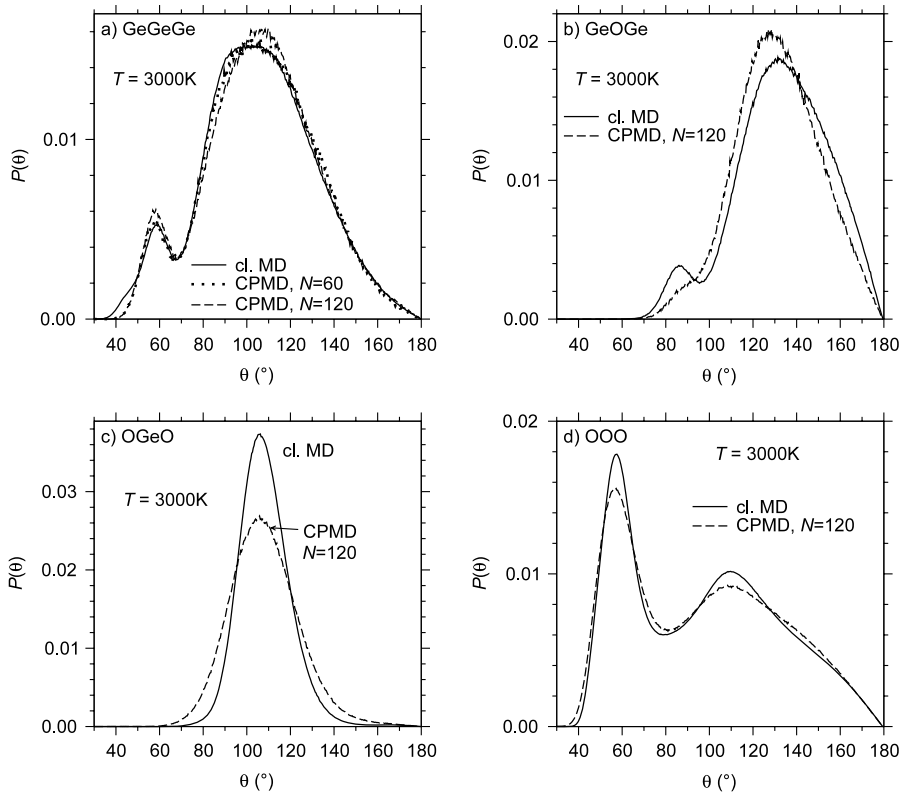

Figure 9. Comparison between MD and CPMD results at $T = 3000$ K for the distribution functions of various angles, Ge–Ge–Ge (a), Ge–O–Ge (b), O–Ge–O (c) and O–O–O (d). All MD results refer to $N = 1152$, while the CPMD are results are for $N = 120$ (for the Ge–Ge–Ge distribution also the CPMD result for $N = 60$ is shown).

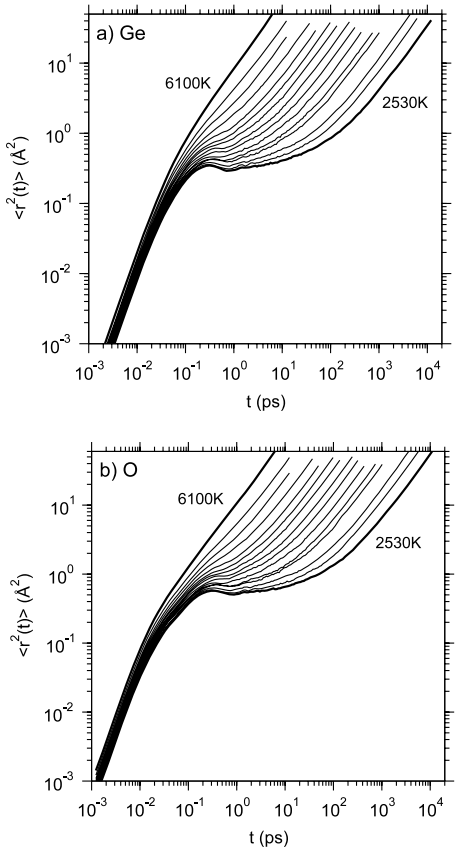

Figure 10. Log–log plot of the MSD for Ge (a) and O (b) versus time for different temperatures. The leftmost curve corresponds to $T = 6100$ K, the rightmost curve to $T = 2530$ K, temperatures in between are 5200, 4700, 4300, 4000, 3760, 3580, 3400, 3250, 3100, 3000, 2900, 2750, and 2640 K.

The MSD allows us to estimate the self-diffusion constants, applying the Einstein relation

$$D_\alpha = \lim_{t\to\infty} \left[\langle r_\alpha^2(t)\rangle/(6t)\right]. \tag{10}$$

Figure 10 shows our MD data for the MSD. One sees the standard behavior, familiar from MD simulations for SiO_2 [15] and many other systems [6]. At very short times, a ballistic regime is seen ($\langle r_\alpha^2(t)\rangle \propto t^2$). Then, at high temperatures, a rapid crossover to the linear diffusive regime occurs ($\langle r_\alpha^2(t)\rangle = 6D_\alpha t$), while at lower temperatures, i.e. in the range 2530 K $\leqslant T \leqslant$ 3250 K, a plateau is observed at intermediate times, where the MSD does not increase, but rather stays constant at about $\langle r_\alpha^2(t)\rangle \approx 0.5$ Å^2. This plateau is commonly interpreted as the onset of the 'cage effect' [3, 6]: each atom sits in a 'cage' formed by its nearest neighbors and the lower the temperature the more time it takes until the atom can 'escape from the cage'. Of course, such mobility implies that the network of bonds in the random network structure is not rigid, sometimes a bond 'breaks' [15] and coordination defects appear, which later can anneal again.

The MSD, as obtained from MD simulation with the OE model, can be also compared to corresponding CPMD results. In figure 11 the MSD for oxygen is displayed in a log–log plot (the MSD for germanium exhibits a similar shape and

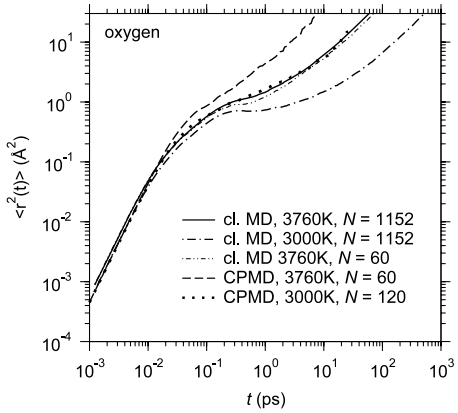

Figure 11. Log–log plot of the MSD for oxygen versus time, comparing classical MD and CPMD results at two temperatures, $T = 3000$ and $T = 3760$ K, and at different system sizes, as indicated. At $T = 3760$ K, the MSD from the classical MD is shown for systems of $N = 60$ and 1152 particles.

is therefore not shown here). The behavior seen in figure 11 is not surprising at all, in view of our findings for static properties as described in detail in the previous section: the time dependence of the MSD found for $T = 3000$ K by CPMD superimposes almost exactly with the MD results for $T = 3760$ K, reinforcing the finding that CPMD is essentially equivalent to the use of pair potentials that are slightly softer than the OE potential but otherwise very similar. As a further caveat we mention the effect of the Nosé–Hoover thermostat (needed in CPMD, not in MD), which may have slightly sped up the CPMD dynamics, though we do not have any real evidence that this effect is already important on time scales up to 20 ps that are shown in figure 11. Also shown in figure 11 is the MSD for oxygen at $T = 3760$ K and $\rho = 3.45$ g cm^{-3}, as obtained from a classical simulation with $N = 60$ particles. This curve indicates that the dynamics becomes slightly slower with decreasing system size (in agreement with our recent finding for SiO_2 [23]). Thus, the higher diffusivity of the atoms in the CPMD simulation cannot be referred to the small system size used in the *ab initio* approach.

In figure 12 a plot of the diffusion constants is presented, choosing a logarithmic ordinate scale and inverse temperature as abscissa, so Arrhenius relations show up as straight lines, since then (compare to equation (1))

$$D_\alpha = D_{\alpha,\infty} \exp[-E_{a,\alpha}/(k_B T)]. \tag{11}$$

The activation energies resulting from the fits in figure 12 are $E_{a,Ge} = 3.41$ eV ± 0.05 eV and $E_{a,O} = 3.25$ eV ± 0.05 eV. As can be also inferred from figure 12, oxygen diffuses slightly faster than Ge, and this difference becomes slightly more pronounced with decreasing temperature, due to the slightly higher activation energy of Ge. A similar behavior is well known for SiO_2 [6, 15].

While in the case of SiO_2 experimental data for self-diffusion constants D_{Si}, D_O are available, we are not aware of suitable data for GeO_2. However, when we disregard the small difference between D_{Ge} and D_O, a rough estimation of these

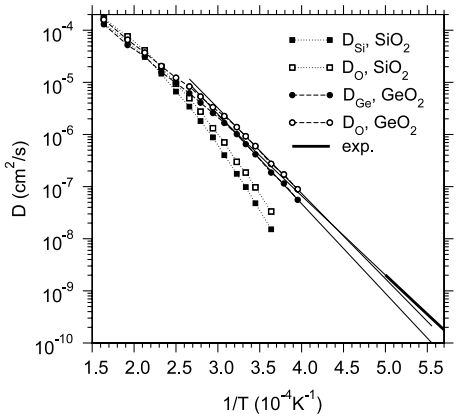

Figure 12. Self-diffusion constants of Ge and O in GeO_2 melts plotted versus inverse temperature. For comparison, results for Si and O in SiO_2 melts (taken from [15]) are included. The dashed and dotted lines serve as a guide to the eye. Straight lines indicate fits to the Arrhenius relation, equation (11). Also an Arrhenius fit resulting from experimental viscosity data [36] via equation (12) is included.

diffusion constants is possible with the well-known Stokes–Einstein relation [6, 81],

$$D = k_B T/[c\pi\eta R], \tag{12}$$

with the constant $c = 4$ if one assumes slip boundary conditions for the particle diffusion in the fluid, η is the shear viscosity of the fluid, and R the radius of the diffusing particle. In principle, equation (12) is a result from hydrodynamics, and makes sense only if R is much larger than interatomic distances. However, in the spirit of the finding that often descriptions based on hydrodynamics work down to the molecular scale (see [85] for a recent example), equation (12) is used also for diffusing atoms or molecules. Then using for R the Ge–O nearest-neighbor distance, $R = 1.75$ Å, the experimental viscosity data of Riebling [36] are readily converted into the self-diffusion constant, and the resulting Arrhenius fit (implying $E_a = 3.565$ eV) is also included in figure 12 and in very good agreement with our simulations.

In contrast to our results, previous simulations [52, 53] gave activation energies in the range between 1 and 1.2 eV. There are many indications that the potential used by Hoang [52] cannot describe GeO_2 as accurately as the OE potential does; moreover his results presumably suffer from aging effects due to insufficient equilibration. The latter criticism also applies to the study of Micoulaut *et al* [53], where the system configurations were taken from one cooling run applying a cooling rate of 2.5×10^{12} K s^{-1}, although states in the temperature range from 940 K $\leqslant T \leqslant$ 2480 K were considered. It is clear that such configurations are far from equilibrium, even at $T = 2940$ K these data [53] do not show any sign of the cage effect, and at the lower temperature ($T = 940$ K), which is only about 100 K higher than the experimental glass transition temperature, the structural relaxation time is only of the order of nanoseconds, which proves that the melt is in a state very far from equilibrium, in the initial stages of aging.

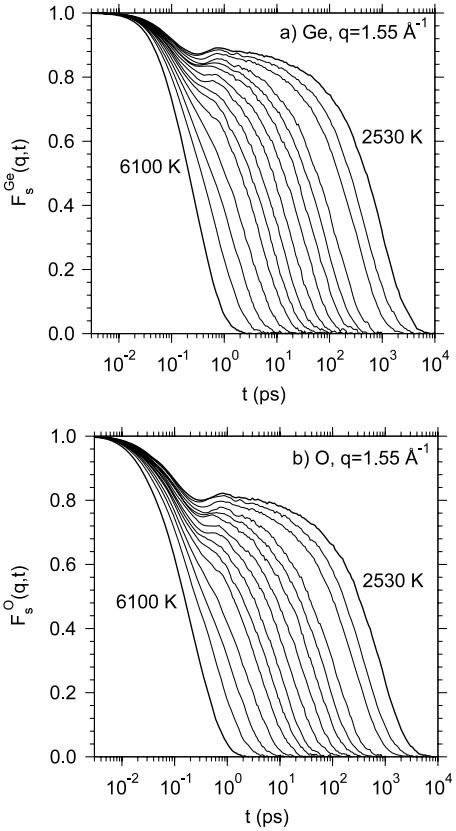

Figure 13. Incoherent intermediate scattering functions $F_s^{Ge}(q,t)$ (a) and $F_s^{O}(q,t)$ (b) for GeO_2 at $q = 1.55$ Å^{-1}, where the static structure factor $S(q)$ exhibits the first sharp diffraction peak, plotted versus time (on logarithmic scale) for a broad range of temperatures (the leftmost curve corresponds to $T = 6100$ K, the rightmost curve to $T = 2530$ K, temperatures in between are 5200, 4700, 4300, 4000, 3760, 3580, 3400, 3250, 3100, 3000, 2900, 2750, and 2640 K).

We now turn to the analysis of intermediate scattering functions (figure 13). Again we note the qualitative similarity of these curves to data for many other glassforming fluids [6, 15]. While at high temperatures the decay of $F_s^\alpha(q,t)$ resembles a simple exponential, for $T \leqslant 3400$ K the decay occurs in two steps, due to the cage effect. The so-called 'β-relaxation' is the time regime around the plateau, while the final decay from this plateau to zero is called 'α-relaxation' [3, 6]. Whereas, at high temperatures $F_s^\alpha(q,t)$ decays to zero on the ps timescale, at the lowest accessible temperatures the 'lifetime' of the plateau already extends into the ns time range. In order to define the structural relaxation time $\tau_\alpha(q,t)$, we follow [17] by requesting that for $t = \tau_\alpha(q,t)$ the scattering function has decayed to a value of 0.1. Thus,

$$F_s^\alpha(q, t = \tau_\alpha(T)) = 0.1, \qquad \alpha = \text{Ge, O}; \tag{13}$$

here we have omitted the argument of the structural relaxation time, since in the present context only the value of q, corresponding to the location of the FSDP in the static structure factor, is of interest.

Figure 14 presents a log–log plot of $\tau_{Ge}(T)$ and $\tau_O(T)$ against $T - T_c$, $T_c = 2490$ K $\pm$ 100 K being an estimate for

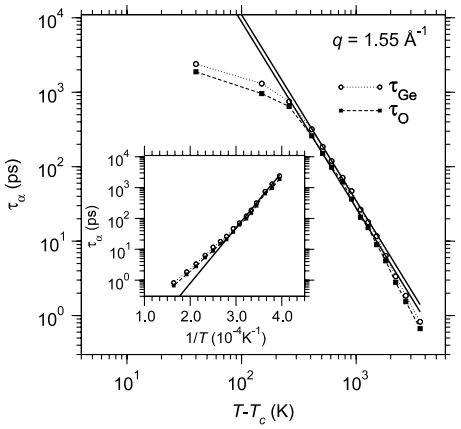

Figure 14. Log–log plot of τ_{Ge} and $\tau_O(T)$ in fluid GeO_2 versus $T - T_c$, using $T_c = 2490$ K. The bold lines are fits with power laws $\propto (T - T_c)^{\gamma}$ using $\gamma = 2.5$. The inset shows the same data as $\log[\tau_\alpha(T)]$ versus $1/T$. The straight line in the inset is a fit with an Arrhenius law ($\propto \exp[E_a/(k_B T)]$) with $E_a = 3.57$ eV.

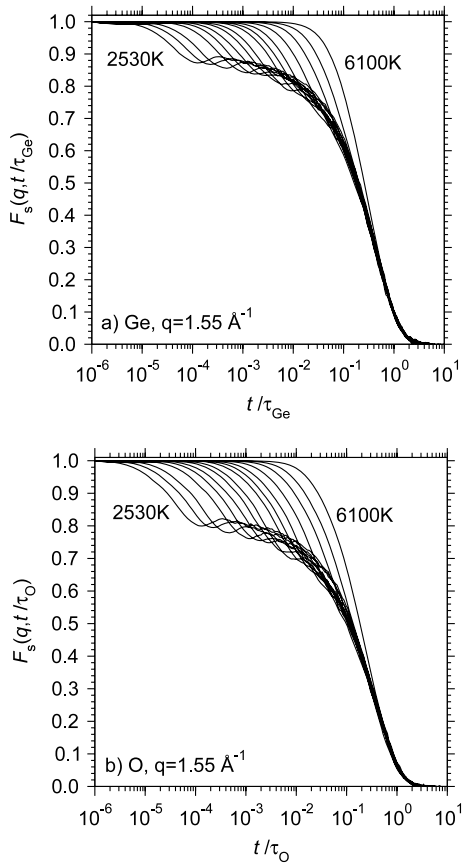

Figure 15. Incoherent intermediate scattering functions $F_s^{\alpha}(q, t)$ plotted versus the scaled time t/τ_α for Ge (a) and O (b). The temperatures shown are the same as those of figure 13.

the mode coupling [3] critical temperature. Of course, it is well known that no real divergence of $\tau_\alpha(T)$, implying an ergodic-to-nonergodic transition and a divergence of the viscosity at T_c, can occur in real glassforming fluids [6]: rather idealized mode coupling theory [3] is a kind of mean field theory for the dynamic correlation functions of glassforming fluids, which supposedly holds for $T > T_c$ but not too close to T_c, since the predicted divergence at T_c is rounded off. The standard albeit heuristic interpretation is that an infinite lifetime of the cage 'imprisoning' of the particles is prevented by thermally activated processes, so-called hopping processes, which break up the cage even for $T = T_c$ and $T < T_c$. So T_c only plays the role of a crossover temperature, where the temperature dependence of $\tau_\alpha(T)$ crosses over from the power law $\tau_\alpha(T) \propto (T - T_c)^{-\gamma}$ to an Arrhenius law. Note that we find the value $\gamma = 2.5 \pm 0.1$ for the critical exponent. This value is slightly higher than the one estimated from simulations of silica [17]. The inset of figure 14 shows that indeed at lower temperatures our estimates for $\tau_\alpha(T)$ are consistent with an Arrhenius law. The activation energy is $E_a = 3.57$ eV $\pm$ 0.05 eV in this case, i.e. slightly higher than those determined for the self-diffusion constants (see figure 12). Of course, this crossover from a power law to thermally activated behavior is by no means sharp, but actually rather gradual, and this smooth behavior near T_c necessarily prevents us from an accurate estimation of T_c: data near T_c may deviate from the straight line on the log–log plot due to the onset of the crossover, even if the estimate for T_c is correct; thus, the precise range of temperatures for which $\tau_\alpha(T)$ should be fitted to the power law is somewhat uncertain, and this leads to a considerable uncertainty about T_c. However, as we can infer from figure 14, the deviations to the mode coupling prediction for $\tau_\alpha(T)$ are small at the lowest simulated temperatures. Thus, we can conclude that the mode coupling prediction for $\tau_\alpha(T)$ essentially holds above about 2500 K.

As further evidence for the applicability of mode coupling theory to describe the dynamics of molten GeO_2 at high temperatures, figure 15 shows a test of the time temperature superposition principle [3, 6]. Of course, the β-relaxation is not supposed to follow this α-scaling and thus the upper part of the curves splay out, while the decay of the plateau (for temperatures where a plateau exists) follows this scaling nicely. The quality with which this scaling holds clearly is comparable to that observed for silica and fragile glassformers.

In SiO_2, Saika-Voivod *et al* [31] have tried to link the relaxation dynamics to structural anomalies, such as the occurrence of a density maximum [31]. These authors have found some evidence for the occurrence of a kind of liquid–liquid phase transition in fluid SiO_2 at suitable conditions of temperature and pressure, i.e. there should exist two phases of fluid SiO_2 with different densities and different structures of the random network of covalent bonds. If this interpretation is correct, figures 12 and 14 would suggest that one should seek a similar interpretation in molten GeO_2, too. However, our data (and the experimental data) for the density of GeO_2 give no hint for the structural anomalies of molten GeO_2 similar to those of SiO_2 (see figure 1).

Finally, we address the question to what extent the Stokes–Einstein relation is valid for germania. In equation (12), this relation was used to link experimental viscosity data [36] to the self-diffusion constants (figure 12). While it would be possible to estimate the shear viscosity from the time-correlation of the off-diagonal pressure tensor components [58, 59], and such an approach has also been shown feasible for molten

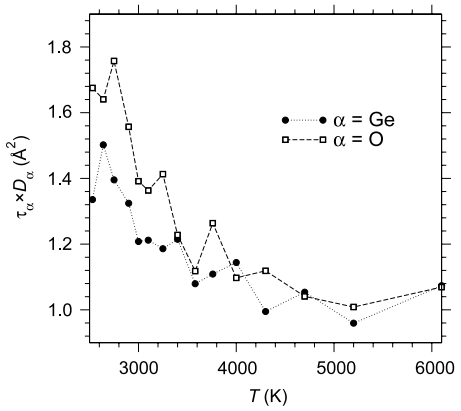

Figure 16. Plot of the product $\tau_\alpha(T)D_\alpha(T)$ versus temperature, for $\alpha =$ Ge and O, as indicated. Simulation results (data points) are connected by lines to guide the eye.

SiO_2 [15], the statistical errors of the resulting estimates are very large. Since one usually associates the shear viscosity with the structural relaxation time, we tentatively tested to what extent the product $\tau_\alpha(T)D_\alpha(T)$ is constant (figure 16). Similarly to SiO_2, where the product $\eta(T)D_\alpha(T)/T$ could be studied [15], one sees some increase of this Stokes–Einstein ratio, but the increase again is not really dramatic. Much more dramatic violations of the Stokes–Einstein relation have been observed for various materials near T_g, and this has received a lot of attention in the literature (see e.g. [14, 86–88]). All of our data are far above the melting temperature of GeO_2, and we can say that in this temperature regime a dramatic breakdown of the Stokes–Einstein relation does not occur. If a breakdown occurs near T_g, this would imply that the good agreement between the experimental data in figure 12 and our estimates for the self-diffusion constants is merely accidental.

5. Conclusions

In the present work, we have described the results of a simulation study of fluid GeO_2 at zero pressure, based on extensive MD runs using the Oeffner–Elliott potential. In the temperature region $T \geqslant 2530$ K the melt has been carefully equilibrated, while glassy structures of amorphous GeO_2 at room temperature were also produced, cooling down the system with two different cooling rates which however produced only minor structural differences. To validate our potential, also an '*ab initio*' Car–Parrinello molecular dynamics (CPMD) study was performed, which is limited to even higher temperatures ($T \geqslant 3000$ K) and very small systems ($N \leqslant 120$ atoms). When we consider properties at small enough scales where systematic errors due to finite size do not matter, we find very good agreement between the MD and CPMD descriptions, for both static and dynamic properties. The most important distinction is that the effective potential to which CPMD corresponds is slightly softer than the OE potential. However, the OE potential is clearly more accurate than other (empirical) potentials that were used in the literature, and our results also agree rather well with the (albeit somewhat scarce) experimental data which are available so far.

Having shown that OE potential is reasonably accurate, it would be interesting to use it both for a more complete study of the dynamics of molten and glassy GeO_2, and for a careful study of GeO_2 under pressure. This must be left to future work. Also it would be interesting to use CPMD to construct a new effective potential which is even more accurate than the OE potential. Such attempts have been made [66], but so far have not been successful.

Our results suggest that for $T \geqslant 2500$ K a crossover sets in for the dynamical properties from a thermally activated behavior of various quantities to a behavior described by mode coupling theory, similar to previous findings for silicon dioxide. In view of our results it is not too surprising that in the temperature range $T \leqslant 1600$ K no experimental evidence for mode coupling effects could be found [42]. Thus, it would be very useful if measurements could be extended to higher temperatures. Also a measurement of self-diffusion constants would be useful, to test the finding that only a rather weak violation of the Stokes–Einstein relation occurs in GeO_2.

GeO_2 and SiO_2 are the two archetypical examples for strong glassformers. Our results imply that they behave qualitatively similar, including the crossover to mode coupling type behavior at temperatures far above melting. The latter crossover is also characteristic for fragile glassformers. However, it is interesting that, in contrast to typical fragile glassformers, the critical mode coupling temperature is above the melting temperature. It has to be seen in future studies whether the relative location of critical temperature and melting temperature can be used as a criterion to distinguish fragile and strong glassformers.

In conclusion, we hope that the present work helps to sort out the many questions concerning the possible universality (or lack thereof) in glassforming fluids, and will stimulate further experimental and theoretical work on the above issues.

Acknowledgments

We thank Th Voigtmann for a critical reading of the manuscript. We are indebted to P S Salmon for providing the experimental data included in the comparison in figure 2. One of us (MH) is grateful to the SCHOTT AG (Mainz) for financial support. We are grateful to U Fotheringham, W Kob and M Letz for stimulating discussions, and acknowledge a substantial grant of computer time at the Jülich multiprocessor system (JUMP) of the John von Neumann Institute for Computing (NIC).

References

[1] Zallen R 1983 *The Physics of Amorphous Solids* (New York: Wiley)
[2] Jäckle J 1986 *Rep. Prog. Phys.* **49** 171
[3] Götze W and Sjögren L 1992 *Rep. Prog. Phys.* **55** 241
[4] Debenedetti P G 1997 *Metastable Liquids* (Princeton, NJ: Princeton University Press)
[5] Angell C A, Ngai K L, Kieffer J, Egami T and Nienhaus G U (ed) 1997 *Structure and Dyamics of Glasses and Glass Formers* (Pittsburg, PA: Material Research Society)

[6] Binder K and Kob W 2005 *Glassy Materials and Disordered Solids: An Introduction to Their Statistical Mechanics* (Singapore: World Scientific)

[7] Andreozzi L, Giordano M, Leporini D and Tosi M (eds) 2007 *Proc. 4th Workshop on Nonequilibrium Phenomena in Supercooled Fluids, Glasses and Amorphous Materials (Pisa, Sept. 2006)*; *J. Phys.: Condens. Matter* **19** (special issue)

[8] Fisher M E 1974 *Rev. Mod. Phys.* **46** 597

[9] Angell C A 1985 *Relaxations in Complex Systems* ed K L Ngai and G B Wright (Springfield: US Department of Commerce)

[10] Götze W 1999 *J. Phys.: Condens. Matter* **11** A1

[11] Biroli G and Bouchaud J-P 2007 *J. Phys.: Condens. Matter* **19** 205101

[12] Franz S and Parisi G 2000 *J. Phys.: Condens. Matter* **12** 6335

[13] Eastwood M P and Wolynes P G 2002 *Europhys. Lett.* **60** 587

[14] Jung Y, Garrahan J P and Chandler D 2004 *Phys. Rev.* E **69** 061205

[15] Horbach J and Kob W 1999 *Phys. Rev.* B **60** 3169

[16] Sciortino F and Kob W 2001 *Phys. Rev. Lett.* **86** 648

[17] Horbach J and Kob W 2001 *Phys. Rev.* E **64** 041503

[18] Angell C A, Clarke J H R and Woodcock L V 1981 *Adv. Chem. Phys.* **48** 397

[19] Rustad J R, Yuen D A and Spera F J 1990 *Phys. Rev.* A **42** 2081

[20] Dellavalle R G and Venuti E 1994 *Chem. Phys.* **179** 411
Dellavalle R G and Venuti E 1996 *Phys. Rev.* B **54** 3809

[21] Tsuneyuki S and Matsui Y 1995 *Phys. Rev. Lett.* **74** 3197

[22] Vollmayr K, Kob W and Binder K 1996 *Phys. Rev.* B **54** 15808

[23] Horbach J, Kob W, Binder K and Angell C A 1996 *Phys. Rev.* E **54** R5897

[24] Pasquarello A and Car R 1997 *Phys. Rev. Lett.* **79** 1766

[25] Horbach J, Kob W and Binder K 1998 *J. Non-Cryst. Solids* **235–238** 320

[26] Horbach J, Kob W and Binder K 1999 *J. Phys. Chem.* B **103** 4104

[27] Jund P and Jullien R 1999 *Phys. Rev. Lett.* **83** 2210

[28] Benoit M, Ispas S, Jund P and Jullien R 2000 *Eur. Phys. J.* B **13** 631

[29] Benoit M, Ispas S and Tuckerman M E 2001 *Phys. Rev.* B **64** 224205

[30] Horbach J, Kob W and Binder K 2001 *Eur. Phys. J.* B **19** 531

[31] Saika-Voivod I, Sciortino F and Poole P H 2001 *Phys. Rev.* E **63** 011202

[32] Shell M S, Debenedetti P G and Panagiotopoulos A Z 2002 *Phys. Rev.* E **66** 011202

[33] Vogel M and Glotzer S C 2004 *Phys. Rev. Lett.* **92** 255901

[34] Takada A, Richet P, Catlow C R A and Price G D 2004 *J. Non-Cryst. Solids* **345/346** 224

[35] Huang L and Kieffer J 2004 *Phys. Rev.* B **69** 224203

[36] Riebling E F 1963 *J. Chem. Phys.* **39** 3022

[37] Fontana E H and Plummer W A 1966 *Phys. Chem. Glasses* **7** 139

[38] Bondot P 1974 *Acta Crystallogr.* A **30** 470
Desa J A E, Wright A C and Sinclair R N 1988 *J. Non-Cryst. Solids* **99** 276
Waseda Y, Sugiyama K, Matsubara E and Harada K 1990 *Mater. Trans. JIM* **31** 421

[39] Dingwell D B, Knoche R and Webb S L 1993 *Phys. Chem. Minerals* **19** 445

[40] Price D L, Saboungi M-L and Barnes A C 1998 *Phys. Rev. Lett.* **81** 3207

[41] Price D L, Ellison A J G, Sabougni M-L, Hu R-Z, Egami T and Howells W S 1997 *Phys. Rev.* B **55** 11249
Neuefeind J and Liss K-D 1996 *Ber. Bunsenges. Phys. Chem.* **100** 1341

[42] Meyer A, Schober H and Neuhaus J 2001 *Phys. Rev.* B **63** 212202

[43] Sampath S, Benmore C J, Lantzky K M, Neuefeind J, Leinenweber K, Price D L and Yarger J L 2003 *Phys. Rev. Lett.* **90** 115502

[44] Ohtaka O, Arima H, Fukui H, Utsumi W, Katayama Y and Yoshiasa A 2004 *Phys. Rev. Lett.* **92** 155506

[45] Salmon P S, Barnes A C, Martin R A and Cuello G J 2006 *Phys. Rev. Lett.* **96** 235502

[46] Salmon P S, Barnes A C, Martin R A and Cuello G J 2007 *J. Phys.: Condens. Matter* **19** 415110

[47] Salmon P S 2007 *J. Phys.: Condens. Matter* **19** 455208

[48] Oeffner R D and Elliott S R 1998 *Phys. Rev.* B **58** 14791

[49] Gutierrez G and Rogan J 2004 *Phys. Rev.* E **69** 31201

[50] Micoulaut M 2004 *J. Phys.: Condens. Matter* **16** L131

[51] Giacomazzi L, Umari P and Pasquarello A 2005 *Phys. Rev. Lett.* **95** 075505

[52] Hoang V V 2006 *J. Phys.: Condens. Matter* **18** 777

[53] Micoulaut M, Guissani Y and Guillot B 2006 *Phys. Rev.* E **73** 031504

[54] Shanavas K V, Garg N and Sharma S M 2006 *Phys. Rev.* B **73** 094120

[55] Giacomazzi L, Umari P and Pasquarello A 2006 *Phys. Rev.* B **74** 155208

[56] Micoulaut M, Cormier L and Henderson G S 2006 *J. Phys.: Condens. Matter* **18** R753

[57] Peralta J, Gutièrrez G and Rogan J 2008 *J. Phys.: Condens. Matter* **20** 145215

[58] Allen M P and Tildesley D J 1987 *Computer Simulation of Liquids* (Oxford: Clarendon)

[59] Binder K and Ciccotti G (ed) 1996 *Monte Carlo and Molecular Dynamics of Condensed Matter* (Bologna: Societa Italiana de Fisica)

[60] Car R and Parrinello M 1985 *Phys. Rev. Lett.* **55** 2471

[61] Marx D and Hutter J 2000 *Modern Methods and Algorithms of Quantum Chemistry* ed J Grotendorst (Jülich: NIC)

[62] http://www.cpmd.org/

[63] van Beest B H W, Kramer G J and van Santen R A 1990 *Phys. Rev. Lett.* **64** 1955

[64] Tsuchya T, Yamanaka T and Matsui M 1998 *Phys. Chem. Minerals* **25** 94

[65] Karthikeyan A and Almeida R M 2001 *J. Non-Cryst. Solids* **281** 152

[66] Hawlitzky M 2006 *Dissertation* Johannes Gutenberg Universität, Mainz

[67] Hawlitzky M, Horbach J and Binder K 2007 *MRS Proc. Symp.* **1048E** Z9.1

[68] Andersen H C 1980 *J. Chem. Phys.* **72** 2384

[69] Goedecker S, Teter M and Hutter J 1996 *Phys. Rev.* B **54** 1703

[70] Troullier N and Martins J L 1991 *Phys. Rev.* B **43** 1993

[71] Martyna G J, Klein M L and Tuckerman M 1992 *J. Chem. Phys.* **97** 2635

[72] Tuckerman M E and Parrinello M 1994 *J. Chem. Phys.* **101** 1302

[73] Mischler C, Kob W and Binder K 2002 *Comput. Phys. Commun.* **147** 222

[74] Mischler C, Horbach J, Kob W and Binder K 2005 *J. Phys.: Condens. Matter* **17** 4005

[75] Sarver J F and Hummel F A 1960 *J. Am. Ceram. Soc.* **43** 336

[76] Kühne T D, Krack M, Mohamed F R and Parrinello M 2007 *Phys. Rev. Lett.* **98** 066401

[77] Vergano P J and Uhlmann D R 1970 *Phys. Chem. Glasses* **11** 30

[78] Angell C A and Kanno H 1976 *Science* **193** 1121

[79] Elliott S R 1992 *J. Non-Cryst. Solids* **150** 112

[80] Price D L and Carpenter J M 1987 *J. Non-Cryst. Solids* **92** 153

[81] Hansen J P and McDonald I R 1990 *Theory of Simple Liquids* (London: Academic)

[82] Tamura T, Lu G-H, Yamamoto R and Kohyama M 2004 *Phys. Rev.* B **69** 195204

[83] Salmon P S 2006 *J. Phys.: Condens. Matter* **18** 11443
[84] Neuefeind J and Liss K-D 1996 *Ber. Bunsenges. Phys. Chem.* **100** 1341
[85] Dimitrov D I, Milchev A and Binder K 2007 *Phys. Rev. Lett.* **99** 054501
[86] Berthier L, Chandler D and Garrahan J P 2005 *Europhys. Lett.* **69** 320
[87] Pan A C, Garrahan J P and Chandler D 2005 *Chem. Phys. Chem.* **6** 1783
[88] Szamel G and Flenner E 2006 *Phys. Rev.* E **73** 011504